Seasonal Kinetic Energy Variability of Near-Inertial Motions

KATHERINE E. SILVERTHORNE

MIT–WHOI Joint Program, Woods Hole, Massachusetts

JOHN M. TOOLE

Woods Hole Oceanographic Institution, Woods Hole, Massachusetts

(Manuscript received 19 September 2007, in final form 25 August 2008)

ABSTRACT

Seasonal variability of near-inertial horizontal kinetic energy is examined using observations from a series of McLane Moored Profiler moorings located at 39°N, 69°W in the western North Atlantic Ocean in combination with a one-dimensional, depth-integrated kinetic energy model. The time-mean kinetic energy and shear vertical wavenumber spectra of the high-frequency motions at the mooring site are in reasonable agreement with the Garrett–Munk internal wave description. Time series of depth-dependent and depth-integrated near-inertial kinetic energy are calculated from available mooring data after filtering to isolate near-inertial-frequency motions. These data document a pronounced seasonal cycle featuring a wintertime maximum in the depth-integrated near-inertial kinetic energy deriving chiefly from the variability in the upper 500 m of the water column. The seasonal signal in the near-inertial kinetic energy is most prominent for motions with vertical wavelengths greater than 100 m but observable wintertime enhancement is seen down to wavelengths of the order of 10 m. Rotary vertical wavenumber spectra exhibit a dominance of clockwise-with-depth energy, indicative of downward energy propagation and implying a surface energy source. A simple depth-integrated near-inertial kinetic energy model consisting of a wind forcing term and a dissipation term captures the order of magnitude of the observed near-inertial kinetic energy as well as its seasonal cycle.

1. Introduction

Oscillations about the inertial frequency f are a commonplace feature of the ocean, with the frequency spectra of most ocean current records tending to display an energetic peak associated with these motions (Fig. 1). The predominant generation mechanism for near-inertial motions is thought to be wind forcing at the ocean surface (e.g., Pollard and Millard 1970; D'Asaro 1985); near-inertial motions can also be forced by geostrophic adjustment. Near-inertial internal waves have a nearly horizontal group velocity and, thus, can propagate energy long distances without encountering the ocean surface or bottom (Garrett 2001). However, wave–wave interactions can lead to energy fluxes into and/or out of the near-inertial frequency band, and dissipation can occur, which acts as a sink for near-inertial energy.

In this paper, we investigate the seasonality of near-inertial internal waves at a site in the western North Atlantic Ocean and examine a localized kinetic energy budget for these motions, focusing specifically on the wind energy input. Because near-inertial motions are so energetic, investigating the near-inertial kinetic energy budget is important from a global perspective. Munk and Wunsch (1998) showed that substantial amounts of energy are needed from the winds and tides to drive the mixing required to maintain the abyssal stratification of the ocean. It has been estimated that the global wind work on inertial motions is comparable to the wind work on geostrophic motions (Alford 2001, 2003). Therefore, investigating the relative importance of the terms in the near-inertial kinetic energy budget contributes to the understanding of the global oceanic energy budget.

Excitation of near-inertial motions by wind forcing has been examined extensively in both modeling and observational studies (e.g., Pollard and Millard 1970; D'Asaro 1985; Plueddemann and Farrar 2006). Time-varying wind stress on the ocean surface can drive inertial mixed layer currents that, in the presence of

Corresponding author address: Katherine Silverthorne, Woods Hole Oceanographic Institution, MS 21, Woods Hole, MA 02543. E-mail: ksilverthorne@whoi.edu

DOI: 10.1175/2008JPO3920.1

© 2009 American Meteorological Society

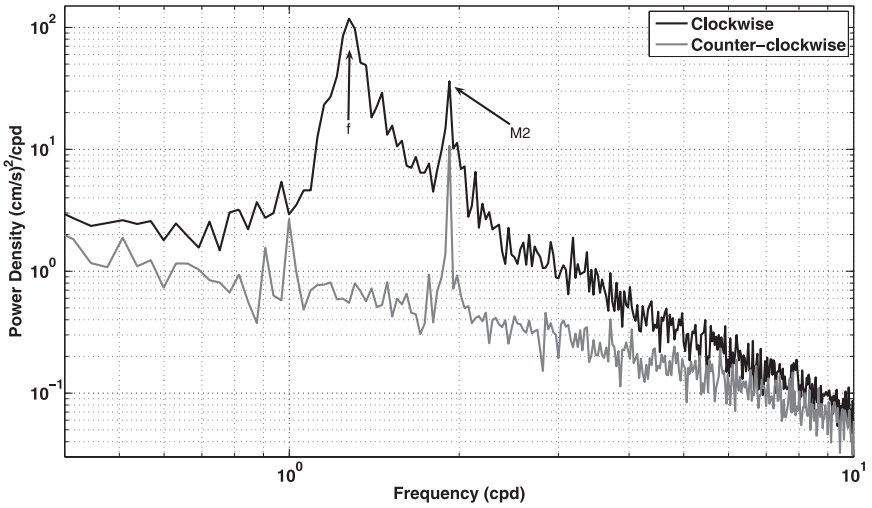

FIG. 1. Rotary frequency spectrum of a Line W vector-averaging current meter record from 39.2°N, 69.4°W and 1000-m depth spanning the time period April 2004–April 2006. The clockwise and counterclockwise components of the spectrum are black and gray, respectively. The spectrum was derived by averaging each periodogram value over 21 neighboring frequency estimates. The inertial peak (frequency = 1.3 cpd) and the M2 tidal peak (frequency = 1.9 cpd) are marked.

spatial inhomogeneities of these currents, can force downward-propagating near-inertial internal waves at the base of the mixed layer. D'Asaro (1985) showed that wind forcing of inertial motions is caused primarily by the passage of storms such as cold fronts and small low pressure systems. Accordingly, there is commonly a winter maximum in the wind energy input into near-inertial motions because of the prevalence of storms in this season (Alford 2001). Recent work by Alford and Whitmont (2007) examined temporal and spatial patterns of near-inertial kinetic energy observed at current meter moorings across the globe. They concluded that there is a surface-intensified, seasonal cycle in near-inertial kinetic energy that is correlated with the estimated wind forcing.

Generation of near-inertial motions by wind forcing has traditionally been studied using the slab model developed by Pollard and Millard (1970). Recent studies have shown that the slab model can overestimate the work done by the wind due to its simple linear parameterization of dissipative processes at the base of the mixed layer (Plueddemann and Farrar 2006). The Price–Weller–Pinkel (PWP) mixed layer model appears to give a better estimate of the work done by the wind because it includes a transition layer below a slablike mixed layer (Price et al. 1986). Vertical transfers of momentum and energy by turbulent mixing governed by a Richardson number criterion and by convection are simulated in the PWP model, allowing the mixed layer depth to evolve, thus making it more realistic than the slab model.

As noted earlier, one possible sink for the energy put into near-inertial motions by the wind is turbulent dissipation due to the interactions of internal waves. Polzin et al. (1995) compared dissipation predictions based on wave–wave interaction models with observations and showed that finescale parameterizations of dissipation in terms of the properties of the internal wave field can accurately capture the observations in regions where internal waves are thought to dominate the mixing (i.e., away from boundaries and large current shear). In particular, the results of their study confirmed the dependence of the dissipation on the buoyancy frequency and the energy level of the internal wave field.

Depth-dependent and depth-integrated time series of near-inertial kinetic energy levels are calculated in this study from observations in the western North Atlantic at 39°N over a 5-yr period. The near-inertial kinetic energy exhibits a strong seasonal cycle with a wintertime maximum, and is dominated by downward energy propagation. A simple kinetic energy model is constructed, and the model results are compared to the observations. It is shown that the kinetic energy model captures the magnitude and seasonal cycle of the near-inertial kinetic energy levels seen in the observations.

2. Observations and analysis procedures

Observations used to calculate the near-inertial horizontal kinetic energy were obtained from a series of moorings fitted with McLane Moored Profilers (MMPs)

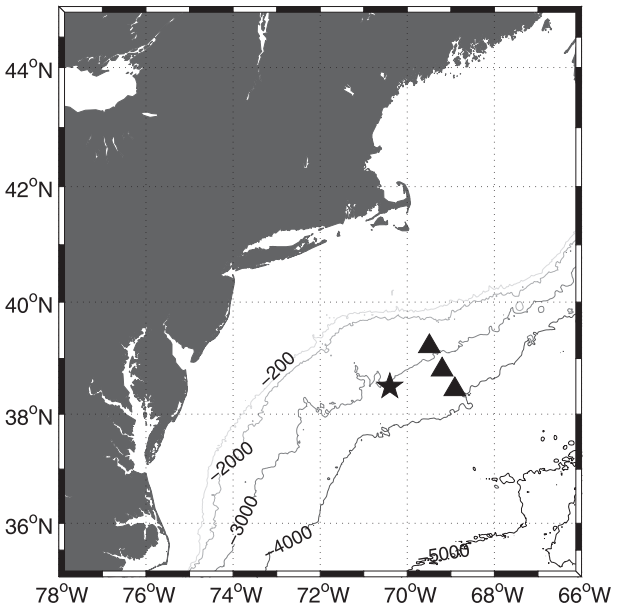

FIG. 2. Map of Line W mooring (triangles) and NDBC buoy (star) locations. The top and bottom triangles mark current meter moorings (W2 and W4, respectively) while the middle triangle indicates the MMP mooring location. Selected isobaths (m) are also displayed.

TABLE 1. MMP deployment details.

	Line W MMP deployments
Location	38.8°N, 69.2°W
Water depth (m)	~3100 m
Instrumentation	CTD: temperature, salinity, pressure ACM: zonal and meridional velocities
Vertical range (m)	75–3000
Vertical resolution (dbar)	2
Temporal range	Four deployments: 3 Nov 2001–14 Aug 2002, 5 Jun 2003–1 May 2004, 10 May 2004–16 Mar 2005, 10 May 2005–5 Apr 2006
Temporal resolution	Burst of four profiles separated by half an inertial period (9.5 h); bursts separated by 4–5 days

located at approximately 38.8°N and 69.2°W in the western North Atlantic Ocean as part of the Line W project (Fig. 2; information online at www.whoi.edu/science/PO/linew/). The details of the MMP deployments are found in Table 1. The MMPs (see Doherty et al. 1999; Toole et al. 1999; Morrison et al. 2000) were programmed to sample in bursts of four near-full-depth (one way) profiles, with initiation of each profile in a burst being separated by half an inertial period and successive bursts separated by 4–5 days. The nominal MMP profile speed is 0.25 m s^{-1}. During each MMP profile, temperature, conductivity, and pressure data are acquired at approximately 1.6 Hz using a low-power CTD, and triaxial velocity and geographic heading data are obtained at comparable rates by an acoustic-travel-time current meter. These raw data were reduced during postprocessing to 2-db bin-averaged estimates of temperature, salinity, and velocity.

Several steps were taken in the analysis of the MMP velocity data in order to extract estimates of the near-inertial kinetic energy. At each depth, the average velocity of the four profiles in each burst was removed to suppress the low-frequency flow signals. The depth mean of each velocity anomaly profile was also removed. The resulting anomaly profiles are thus dominated by high-frequency, depth-varying motions believed to consist chiefly of internal waves, and are referred to as ''super-inertial motions'' in the following. Estimates of the near-inertial horizontal velocity profile (u_i, v_i) for each burst were derived from a linear combination of the four anomaly profiles as follows:

$$u_i = 0.25(u_1 - u_2 + u_3 - u_4) \quad \text{and}$$
$$v_i = 0.25(v_1 - v_2 + v_3 - v_4), \tag{1}$$

where (u_1, v_1) is the first velocity anomaly profile in a burst, (u_2, v_2) is the second velocity anomaly profile in the burst, and so on. This inertial filtering technique, discussed in detail in appendix A, takes advantage of the fact that the ratio of the inertial period to the M2 tidal period at the mooring latitude is 1.5 to filter semidiurnal tidal energy. The near-inertial kinetic energy profile for each burst (KE_i) was calculated as follows:

$$\mathrm{KE}_i = \frac{1}{2}\rho_o(u_i^2 + v_i^2), \tag{2}$$

where ρ_o is the reference density (here defined as 1024 kg m^{-3}). When performing depth integration of the near-inertial kinetic energy, missing values (such as those that occur when the MMP fails to profile fully between the top and bottom stops on the mooring wire) were assumed to be zero, thus yielding a lower-bound estimation.

Because the near-inertial kinetic energy is expected to vary with the buoyancy frequency N to first order, it is necessary to apply Wentzel–Kramers–Brillouin (WKB) scaling to remove this dependence (Leaman and Sanford 1975). The superinertial and near-inertial kinetic energy profiles were therefore WKB scaled using buoyancy frequency estimates derived from time-averaged MMP measurements of temperature, salinity, and pressure, and from the standard N_o value of 3 cph. Rotary vertical

wavenumber spectra of the WKB-scaled velocity profiles were calculated for the depth range of 200–500 m to infer the sense of vertical energy propagation. The mean value of the buoyancy frequency was 2 cph and varied little over that depth range. Examination of vertical wavenumber spectra of the full MMP observed velocity profiles during summertime indicated that the spectra began to level out (indicating noise) at vertical wavelengths smaller than 10 m. Integrating this inferred noise level across wavenumber space gives an estimate of the MMP RMS velocity error as 0.7 cm s^{-1}.

3. Results

a. Representative velocity profiles and average vertical wavenumber spectra

The derived superinertial anomaly velocity profiles often display the mirror imaging previously observed in velocity measurements separated by half an inertial period (Fig. 3). Clockwise rotation with depth of the near-inertial velocity vector is evident in the estimated near-inertial velocity components (Fig. 3, right column). Of the three examples presented, the typical summertime velocity profiles are the smallest in magnitude and also do not exhibit much variation with depth (Fig. 3, top row). In contrast, the typical wintertime velocity profiles display a strong intensification in the upper 500 m of the water column (Fig. 3, middle row). Velocity profiles estimated during the winter of 2001/02 demonstrate unusually large magnitudes at depths below 500 m (Fig. 3, bottom row).

The average vertical wavenumber kinetic energy and shear spectra based on all available velocity anomaly profiles (Figs. 4 and 5) are in good agreement with the Garrett–Munk model (Munk 1981). The shape of the near-inertial kinetic energy spectrum closely parallels that of the full superinertial spectrum and accounts for much of the magnitude of the latter. Both the superinertial and the near-inertial vertical wavenumber shear spectra are blue for vertical wavenumbers less than 10^{-2} cpm and nearly white over the vertical wavenumber range from 10^{-2} to 10^{-1} cpm, with the spectra being dominated by noise at vertical wavenumbers greater than 10^{-1} cpm. Rotary vertical wavenumber spectra of the WKB-scaled near-inertial velocity show that the near-inertial motions are dominated by clockwise turning with depth motions at vertical scales larger than 100 m (Fig. 6). (Clockwise turning is indicative of the dominance of low-frequency internal waves carrying energy downward.) This assessment holds true for both summertime and wintertime data subsets. However, the clockwise wintertime near-inertial motions contain more energy at larger vertical scales than the summertime clockwise near-inertial motions.

b. Seasonality of kinetic energy

Consistent with expectations based on prior work, a seasonal cycle of the near-inertial motions is observed with enhanced depth-integrated kinetic energy in winter and minimum energy in summer (Fig. 7). Depth–time contour plots of the super- and near-inertial kinetic energy (Figs. 8 and 9) reveal that the bulk of the winter enhancement of the depth-integrated superinertial and near-inertial kinetic energy derives from depths of less than 500 m: the principal exception being the strong event in the winter of 2001/02, which reached below 3000 m. Observations of the mixed layer depth (when available) demonstrate that the wintertime maxima of the near-inertial kinetic energy consistently extended well below the mixed layer base. Although the WKB-scaled super- and near-inertial kinetic energies contain less variation with depth than their unscaled counterparts, they are nevertheless dominated by the strong, surface-intensified seasonal pulses (Figs. 8 and 9, bottom panels). The wintertime enhancement and surface intensification can be seen more clearly in seasonally averaged profiles of observed superinertial and near-inertial kinetic energy (Figs. 10 and 11). The time-averaged near-inertial kinetic energy profile is similar in shape and only slightly smaller in magnitude than the total superinertial kinetic energy profile. The summertime near-inertial kinetic energy profile is nearly uniform with depth, whereas the wintertime near-inertial kinetic energy displays statistically signified enhancement in the upper portion of the water column. (Confidence bounds at the 95% significance level were derived based on the 10-day decorrelation time scale for the interseasonal kinetic energy time series suggested by analysis of autocorrelation functions.) Alford and Whitmont (2007) observed surface-intensified enhancement of wintertime WKB-scaled near-inertial kinetic energy with a decay in energy from 500- to 3500-m depth by a factor of 3–4; here, we observe a decay of approximately a factor of 2 from 500- to 3200-m depth. In contrast, the WKB-scaled near-inertial kinetic energy in January–March 2002 was nearly constant in depth due to anomalous deep energy. The enhanced near-inertial energy below 1200-m depth appeared approximately 2 weeks after the start of a surface-intensified energy pulse and lasted for over 2 weeks.

4. Discussion

Examination of the observed superinertial and near-inertial kinetic energy reveals the following notable

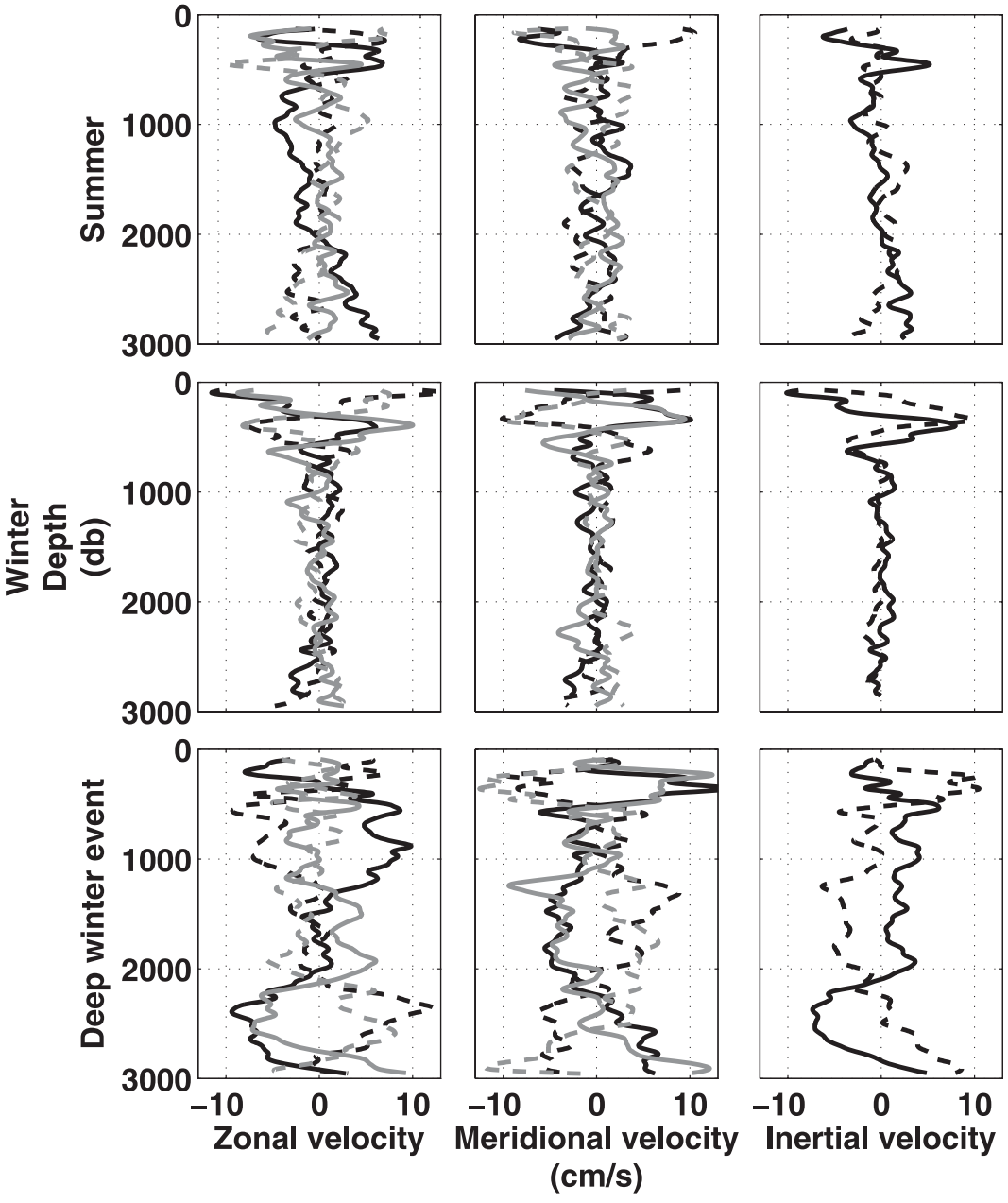

FIG. 3. MMP anomaly velocity depth profiles in cm s^{-1} that have been smoothed with a running depth mean of 50 m. (top row) Data from a typical summer burst (observed in June 2002), (middle row) data from a typical winter burst (observed in January 2004), and (bottom row) data from the anomalous winter deep event (observed in February 2002) are shown. For the (left) zonal velocities and (middle) meridional velocities where the solid black line represents the first burst profile, the dashed black line represents the second burst profile, the solid gray line represents the third burst profile, and the dashed gray line represents the fourth burst profile. (right) The zonal (solid black line) and meridional (dashed black line) inertial velocity components shown were calculated using the linear combination scheme.

feature: a marked seasonal cycle with a winter maximum most pronounced in the upper 500 m of the water column. The surface intensification of the near-inertial kinetic energy, along with the dominance of downward-propagating near-inertial energy at large vertical scales, endorse the hypothesis that near-inertial internal waves in this region are chiefly surface forced. Furthermore, the seasonal cycle in the observed near-inertial kinetic energy supports the idea that the near-inertial motions are predominantly forced by the passage of winter

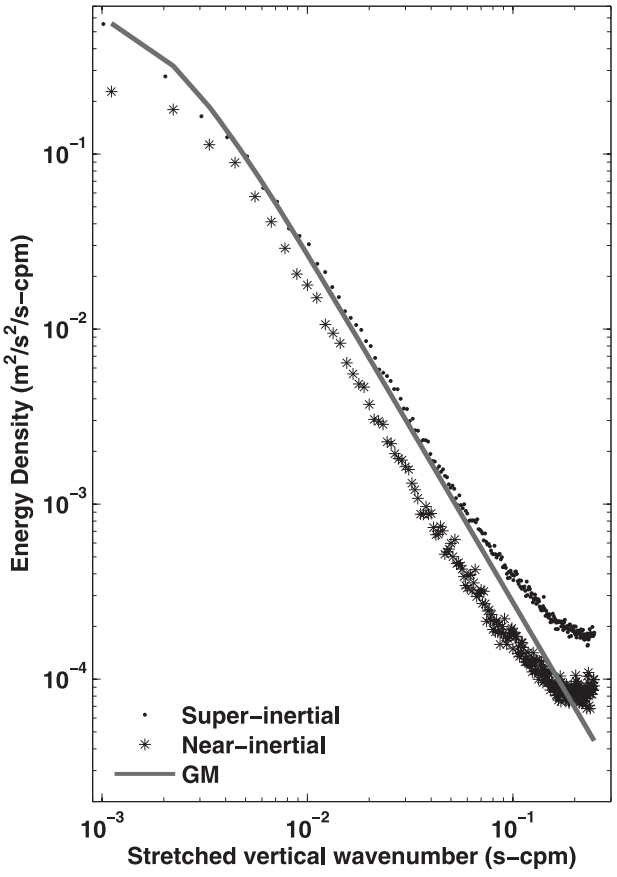

FIG. 4. Observed WKB-scaled superinertial (diamonds) and near-inertial (stars) vertical wavenumber kinetic energy spectra with the Garrett–Munk model (gray line) for jstar (mode number) = 5. The superinertial vertical wavenumber kinetic energy spectrum was calculated as the mean of periodograms estimated from 360 velocity anomaly profiles, while the near-inertial kinetic energy vertical wavenumber spectrum was calculated as the mean of periodograms derived from 78 near-inertial velocity profiles.

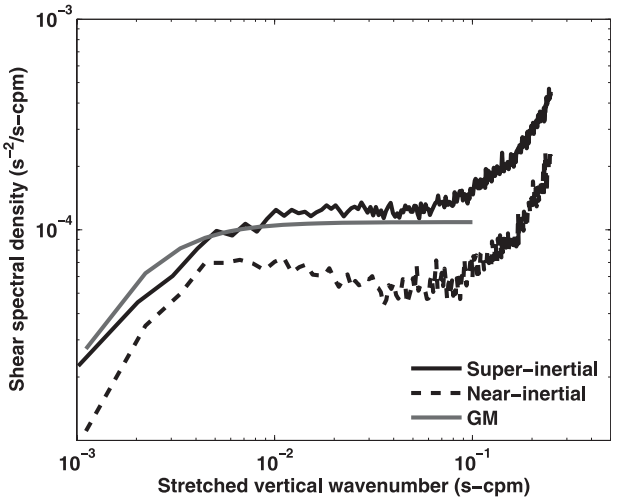

FIG. 5. Observed WKB-scaled superinertial (black line) and near-inertial (black dotted line) vertical wavenumber shear spectra with the Garrett–Munk model (gray line) for jstar = 5. The shear spectra were derived as the product of the velocity spectra (Fig. 4) and the square of the vertical wavenumber.

storms, as was concluded by Alford and Whitmont (2007).

To further develop the idea that winter storms are responsible for the observed seasonal signal, we constructed a simple local kinetic energy model for the near-inertial motions. Invoking an eddy-viscosity closure approximation, the horizontal momentum equations were bandpassed over the near-inertial frequency band, yielding the following:

$$\frac{\partial}{\partial t}u_i + \langle \mathbf{u}\cdot\nabla u\rangle - fv_i = -\frac{1}{\rho_o}\frac{\partial}{\partial x}P_i + A\frac{\partial^2}{\partial z^2}u_i \quad \text{and} \tag{3a}$$

$$\frac{\partial}{\partial t}v_i + \langle \mathbf{u}\cdot\nabla v\rangle + fu_i = -\frac{1}{\rho_o}\frac{\partial}{\partial y}P_i + A\frac{\partial^2}{\partial z^2}v_i, \tag{3b}$$

where A is the eddy viscosity, (u_i, v_i) is the near-inertial velocity, P_i is the near-inertial pressure, and the angled brackets represent the near-inertial bandpass filter. Equations (3a) and (3b) were then multiplied by the zonal and meridional components of the near-inertial velocity, respectively; added together; multiplied by density; and integrated in depth to produce an equation governing the near-inertial kinetic energy:

$$\underbrace{\frac{\partial}{\partial t}\int_{-B}^{0}\mathrm{KE}_i dz}_{\text{I.}} = \underbrace{\mathbf{u}_i\cdot\boldsymbol{\tau}_i|^0}_{\text{II.}} - \underbrace{\int_{-B}^{0}\nabla\cdot(\mathbf{u}_i P_i)dz}_{\text{III.}} - \underbrace{\rho_o\int(u_i\langle\mathbf{u}\cdot\nabla u\rangle + v_i\langle\mathbf{u}\cdot\nabla v\rangle)dz}_{\text{IV.}} - \underbrace{A\int_{-B}^{0}\left[\left(\frac{\partial}{\partial z}u_i\right)^2 + \left(\frac{\partial}{\partial z}v_i\right)^2\right]dz}_{\text{V.}}, \tag{4}$$

where B represents the water depth, and the near-inertial bandpass-filtered wind stress τ_i has been introduced using the expression $\rho_o A(\partial/\partial z\, u_i,\ \partial/\partial z\, v_i) = \boldsymbol{\tau}_i$. Also, the bottom stresses have been assumed to be small compared to the other terms. Neither the spatial nor the temporal resolutions of the early Line W moored measurements were sufficient to estimate the phase of the inertial motions or horizontal gradients, so the

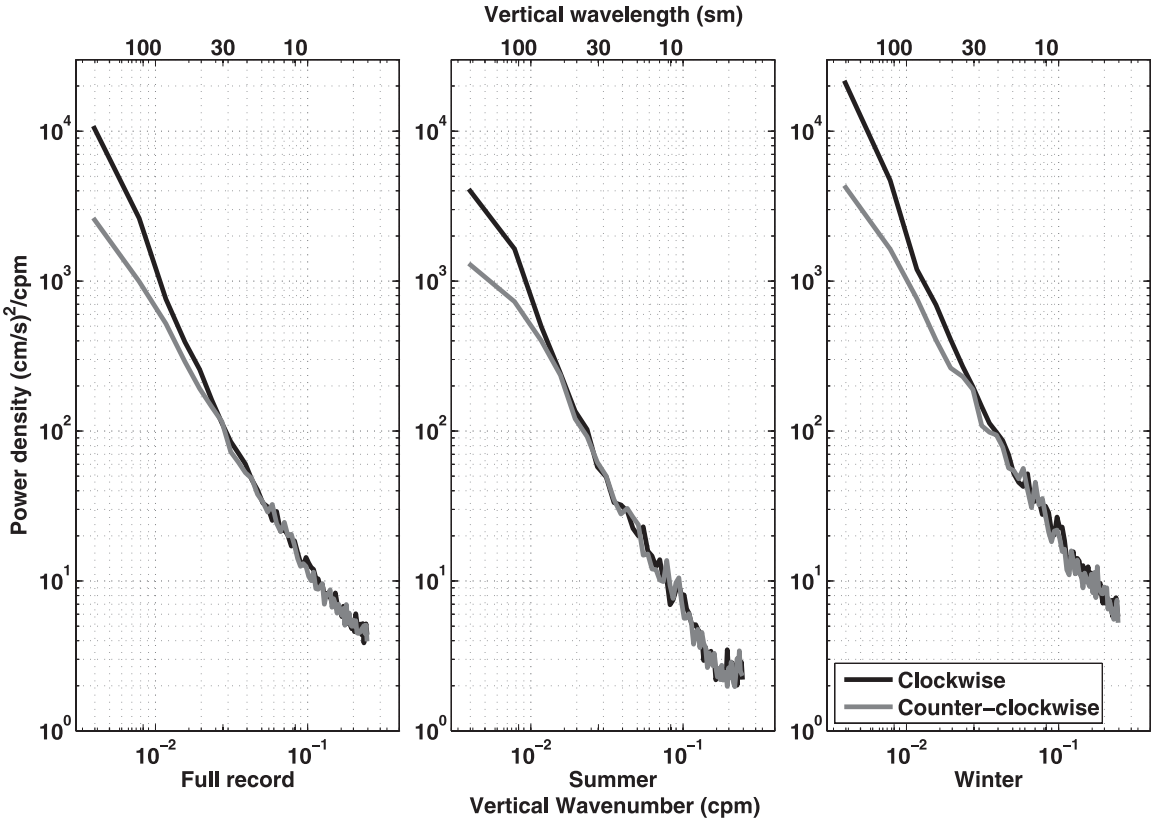

FIG. 6. Rotary vertical wavenumber spectra of the WKB-scaled near-inertial velocity profiles showing the clockwise turning with depth component (black line) and the counterclockwise component (gray line). The (left) full near-inertial kinetic energy spectrum, (middle) summertime near-inertial kinetic energy spectrum, and (right) wintertime near-inertial kinetic energy spectrum were calculated as the mean of 214, 63, and 66 velocity periodograms, respectively, for the depth interval of 200–500 m. The top axis shows the WKB-stretched vertical wavelength derived using a N_o value of 3 cph.

energy flux divergence term (III) could not be estimated. If the near-inertial internal wave energy consists of bursts of wave packets, one might expect that the energy flux divergence term during individual storm events would not be negligible as these packets propagated past the MMP mooring. Indeed, D'Asaro et al. (1995) showed that during the Ocean Storms experiment the observed decay of near-inertial energy out of a region after a storm was consistent with the predicted horizontal internal wave propagation. However, given a random forcing and wave field, the average horizontal energy flux at long time scales (and in turn its divergence) should be close to zero. One possible flaw in this reasoning is the location of the MMP on the continental

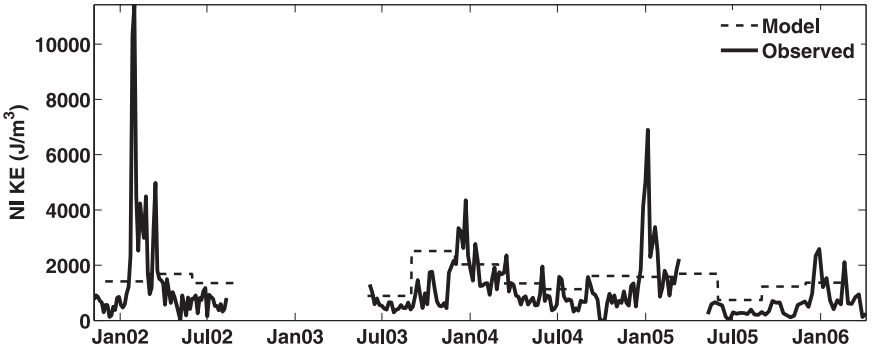

FIG. 7. Depth-integrated near-inertial kinetic energy from observations (black line) and model (thin-dashed line) in J m^{-3}. The model results shown are seasonal averages.

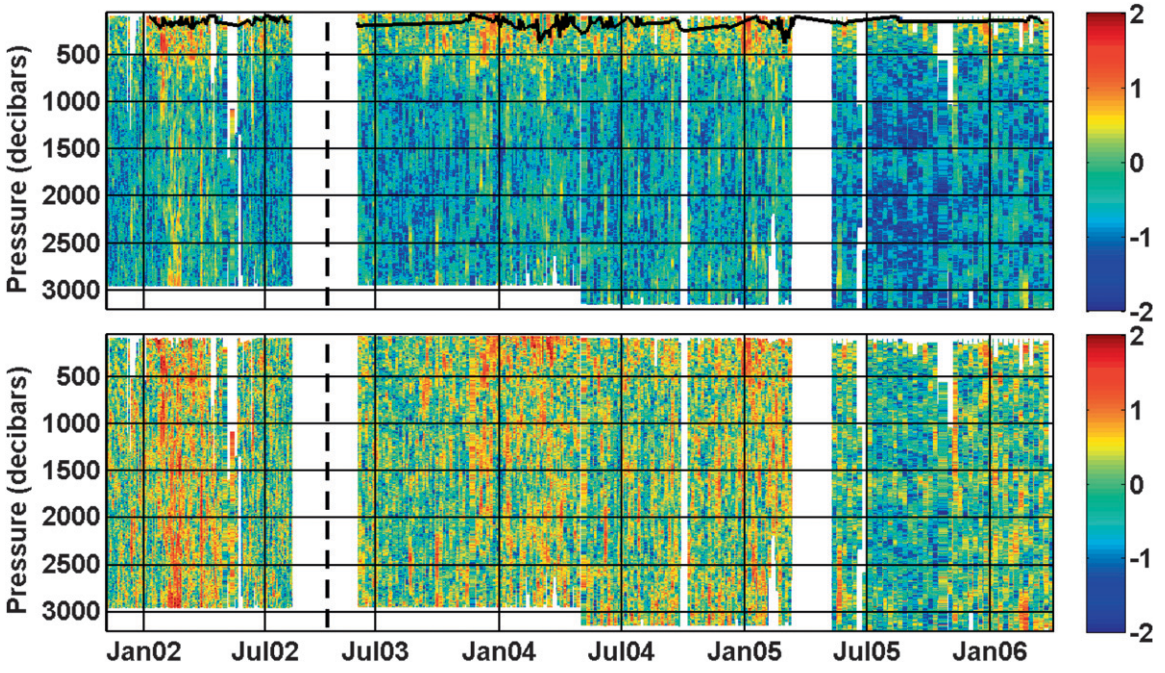

FIG. 8. (top) Depth–time contour plot of the log of the observed superinertial kinetic energy in J m^{-3}. The black solid line represents the MMP-observed mixed layer depth (when available). (bottom) Depth–time contour plot of the log of the WKB-scaled observed superinertial kinetic energy in J m^{-3}. The black dotted lines mark a jump in the time axis.

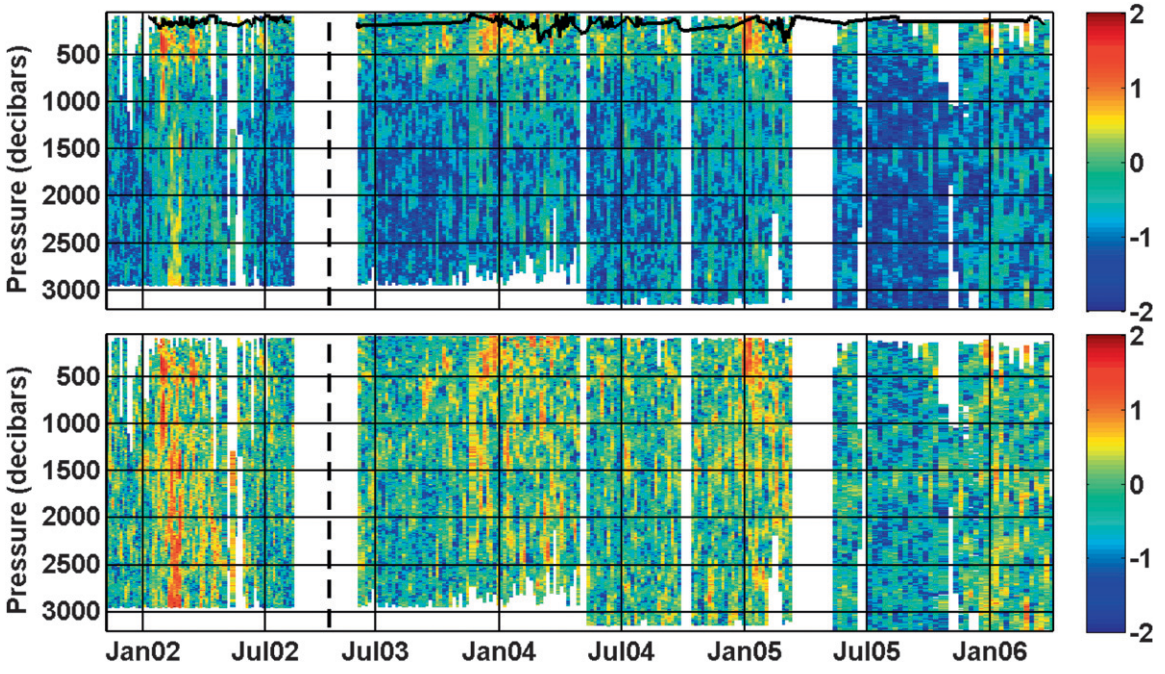

FIG. 9. (top) Depth–time contour plot of the log of the observed near-inertial kinetic energy in J m^{-3}. The black solid line represents the MMP observed mixed layer depth (when available). (bottom) Depth–time contour plot of the log of the WKB-scaled observed near-inertial kinetic energy in J m^{-3}. The black dotted lines mark a jump in the time axis.

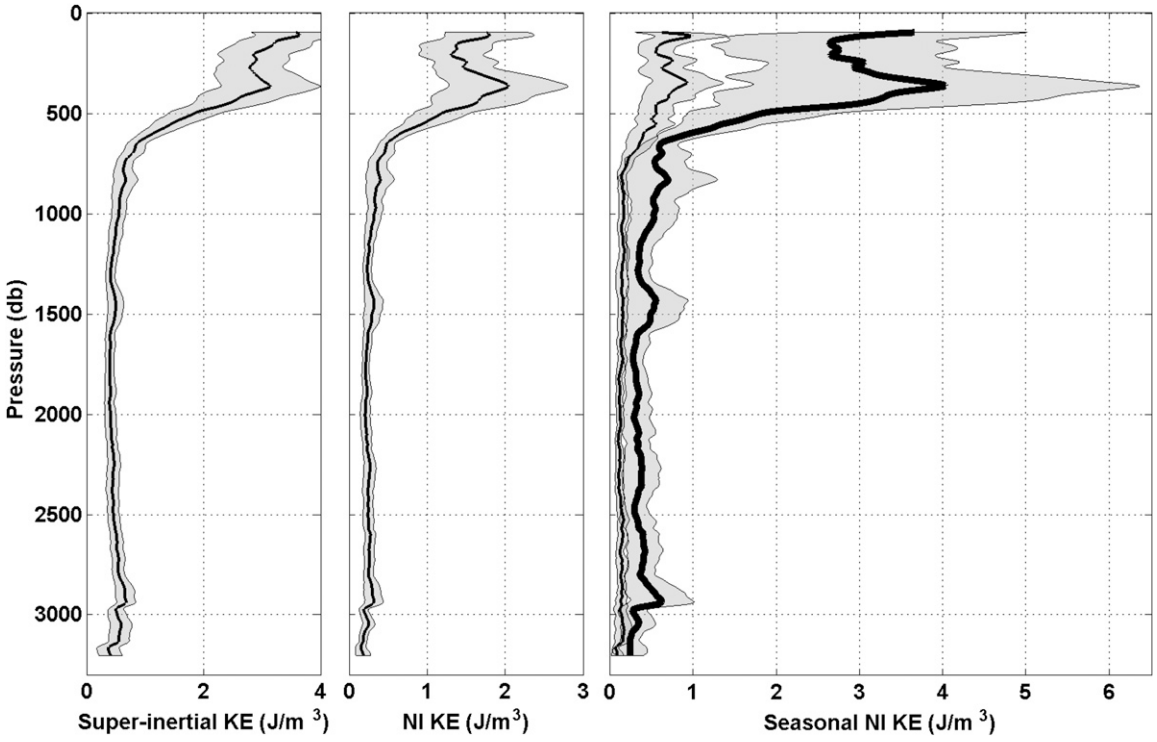

FIG. 10. Observed time mean kinetic energy profiles with 95% confidence intervals calculated by assuming the use of a decorrelation time scale of 10 days. Profiles have been smoothed with a running mean over 20 m. (left) The superinertial kinetic energy profile, (middle) the near-inertial kinetic energy profile, and (right) the summertime (thinner black line) and wintertime means (thicker black line) are shown. The summertime mean was derived using values from June to August, while the wintertime mean was derived using values from December to February.

slope, approximately 100 km from the shelf break, which could mean that the internal wave field has a preferred direction and the energy flux divergence does not average out to zero.

The wind work term (II) was estimated using the PWP mixed layer model, as described in appendix B, and introduced into the kinetic energy model as a prescribed forcing term. Term IV on the right-hand side of the kinetic energy equation represents the transfer of energy between the near-inertial band and motions of other frequencies, while term V takes the form of a viscous dissipation, with the parameterized eddy viscosity (A) in place of the traditional molecular viscosity. Focusing on vertical scales of order 100 m (which characterize the observed seasonal near-inertial signal), we neglect term V with respect to term IV, arguing that the latter represents the principal transfer of energy to smaller vertical scales where it is presumed to dissipate. (However, term V may contribute in the surface mixed layer; see below.) The wave–wave interaction term was parameterized as a turbulent dissipation in terms of the kinetic energy itself, making the model nonlinear. The near-inertial kinetic energy was initially set to zero, and the model was stepped forward in time using a forward difference scheme at an hourly time step, solving for the depth-integrated kinetic energy (I).

Random superposition of internal waves can lead to enhanced shear levels, which are associated with wave breaking and subsequent mixing, and therefore the turbulent dissipation due to wave–wave interactions is dependent on the characteristics of the internal wave field. Gregg (1989) and Polzin et al. (1995) determined that the turbulent kinetic energy dissipation rate ε can be expressed in terms of the buoyancy frequency N, base level kinetic energy E_o, and the internal wave energy level E as

$$\varepsilon = 7 \times 10^{-10} \left(\frac{N}{N_o}\right)^2 \left(\frac{E}{E_o}\right)^2 (\mathrm{W\ kg^{-1}}), \qquad (5)$$

which is consistent with the dynamical models introduced by Henyey et al. (1986) and McComas and Muller (1981). This equation was substituted for term IV in the near-inertial kinetic energy in Eq. (4) under the assumption that the dissipation is local in frequency space, that is, that the loss rate of near-inertial kinetic energy by wave–wave interactions is dependent on the near-inertial internal wave energy level. Inspection of

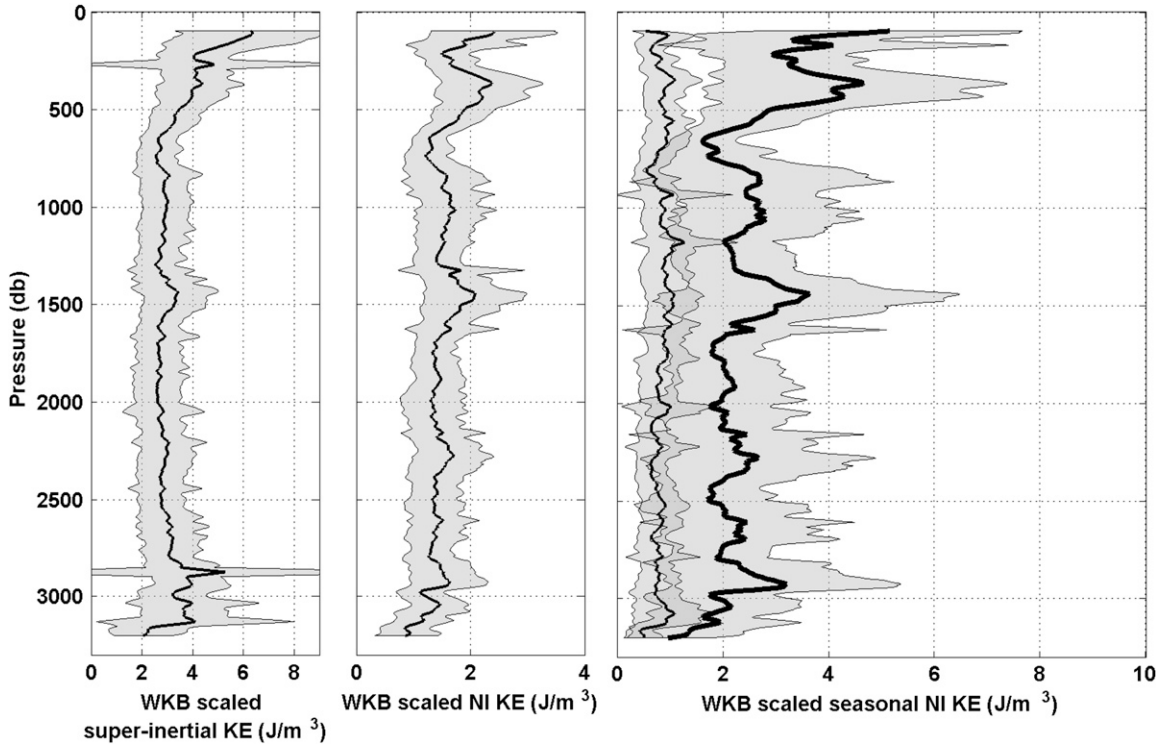

FIG. 11. WKB-scaled time-mean kinetic energy profiles with 95% confidence intervals calculated using a decorrelation time scale of 10 days. Profiles have been smoothed with a running mean over 20 m. (left) The superinertial kinetic energy profile, (middle) the near-inertial kinetic energy profile, and (right) the summertime (thinner black line) and wintertime means (thicker black line) are shown. The summertime mean was derived using values from June to August, while the wintertime mean was derived using values from December to February.

the MMP observations indicates that the near-inertial and the superinertial kinetic energy have similar shape in vertical wavenumber space and variations in time, implying that they are proportional. Therefore, the parameterization of the dissipation of near-inertial kinetic energy as in Eq. (5) is consistent with the behavior of the observed internal wave field. The buoyancy frequency, N, in (5) was calculated as the time and depth mean of the buoyancy frequency for all of the MMP profiles, and the base-level kinetic energy E_o was taken as the summertime (June–August) mean of the observed depth-integrated near-inertial kinetic energy.

The depth-integrated near-inertial kinetic energy model (consisting of the wind input term given as $\mathbf{u}_i \cdot \boldsymbol{\tau}_i$ and a dissipation term governed by widely accepted finescale parameterizations of internal wave decay) gives a prediction for seasonal-mean KE that is within a factor of 2.5 of the observations and also captures the observed wintertime enhancement (Fig. 7). Inspection of the individual terms of the kinetic energy model showed that at long periods, the time rate of change of the depth-integrated near-inertial kinetic energy is small, and therefore the dissipation term is nearly equal and opposite to the wind forcing term on seasonal time scales. The ability of the depth-integrated near-inertial kinetic energy model to capture the seasonal cycle seen in the observations implies that on long time scales there might exist a balance between wind work on near-inertial motions and the loss of internal wave energy through breaking and, ultimately, turbulent dissipation.

The use of Eq. (5) to represent the dissipation in the kinetic energy model carries an inherent assumption that all the work done by the near-inertial wind is radiated into the ocean interior as internal waves whose energy is, in turn, transferred to small vertical scales and eventually dissipated. Even though it is expected that some fraction of the work done by the wind on mixed layer inertial motions is dissipated locally in the mixed layer, it is difficult to determine what that fraction is. Skyllingstad et al. (2000) carried out an LES simulation with (spatially uniform) inertially resonant forcing that suggests that as much as half of the wind input into inertial motions is dissipated in the mixed layer. Thus, for comparison, the kinetic energy model was run with the wind energy forcing term reduced by half. Reducing the

TABLE 2. Horizontal radius of influence (in km) for various near-inertial frequencies.

Frequency	1.005*f*	1.01*f*	1.05*f*	1.1*f*	1.15*f*	1.2*f*
Angle with horizontal (°)	0.11	0.15	0.35	0.50	0.62	0.72
Horizontal radius of influence (km)	264	186	82	58	47	40

wind forcing by half reduces the predicted time-mean near-inertial kinetic energy level by a factor of 1.4. In addition, a third run was conducted in which the forcing was derived from the linear drag term of the PWP model (the term included in PWP to simulate the radiation of energy out of the mixed layer into the stratified interior). Using the PWP drag forcing term results in a slight reduction of the predicted time-mean near-inertial kinetic energy level by a factor of 1.1. All three of the model runs capture the seasonal cycle with maximum energy in winter. Comparison of the modeled seasonal cycle of near-inertial kinetic energy with the observations indicates that the root-mean-square errors for all the model runs are within 70 J m^{-3} of each other, with the half wind forcing model run and the drag forcing model run having slightly smaller errors than the full model run.

However, the model shows little to no skill in capturing individual energetic events in the record; clearly propagation/advection effects are significant at shorter time scale. The largest observed depth-integrated near-inertial kinetic energy was recorded in the winter of 2001/02, and corresponded with the presence of enhanced near-inertial kinetic energy at greater depths than in other years. Examination of the MMP observed temperature as well as satellite SST maps indicates that a warm core Gulf Stream ring was in the vicinity of Line W during the measured deep event. Warm core Gulf Stream rings can trap near-inertial internal waves, leading to increased energy levels (Kunze et al. 1995) and, therefore, could be responsible for the anomalous deep event.

The observation that the seasonal enhancement of near-inertial horizontal kinetic energy was most evident above 500-m depth was used to estimate the horizontal extent of the surface forcing responsible for the near-inertial energy observed at the MMP mooring site (Table 2). Assuming a range of internal wave frequency values covering from 1.005*f* to 1.2*f*, and estimating the mean *N* value spanning 75 to 500 m from all four MMP mooring deployments, the internal wave dispersion relation was used to calculate the angle of the internal wave group velocity vector with the horizontal. Applying the fact that the vertical extent of the enhanced energy was 500 m yields a horizontal radius of influence that varies from ~260 to ~40 km. Any anomalously strong near-inertial energy packet that is generated farther away than the calculated radius of influence in any direction from the mooring site presumably dissipates before reaching the mooring site, or else it would be visible below 500-m depth.

There are several ways this study could be improved upon. Increasing the sampling frequency of the MMP would be advantageous in two ways: 1) it would better resolve the near-inertial frequency motions and 2) it would allow for the estimation of the horizontal energy flux. In turn, adding a coherent array of profilers would be useful for examining the energy flux divergence, and investigating the balances between the terms in the kinetic energy equation on an individual wind event basis. Measuring wind speed and surface velocity at the mooring site would allow for the more accurate estimation of the wind energy input term.

Acknowledgments. Funding to initiate the McLane Moored Profiler observations at Line W were provided by grants from the G. Unger Vetlesen Foundation and the Comer Charitable Fund to the Woods Hole Oceanographic Institution's Ocean and Climate Change Institute. Ongoing moored observations at Line W are supported by the National Science Foundation (NSF Grant OCE-0241354). Any opinions, findings, and conclusions or recommendations expressed in this material are those of the authors and do not necessarily reflect the views of the National Science Foundation. Thanks to Tom Farrar for his insight on implementing the PWP model and calculating the wind work on inertial motions.

APPENDIX A

Estimation of Near-Inertial Motions

The MMP burst sampling scheme was exploited to calculate the near-inertial velocity as a linear combination of the burst velocity anomaly profiles as in Eq. (1). This scheme provides one estimate of the near-inertial velocity profile for each burst, and takes advantage of the fact that the ratio of the inertial period to the M2 tidal period at this latitude is ~1.5 to filter out M2 tidal energy. The calculation of near-inertial velocity with this method is sensitive to the phase of the near-inertial motions that have been sampled. However,

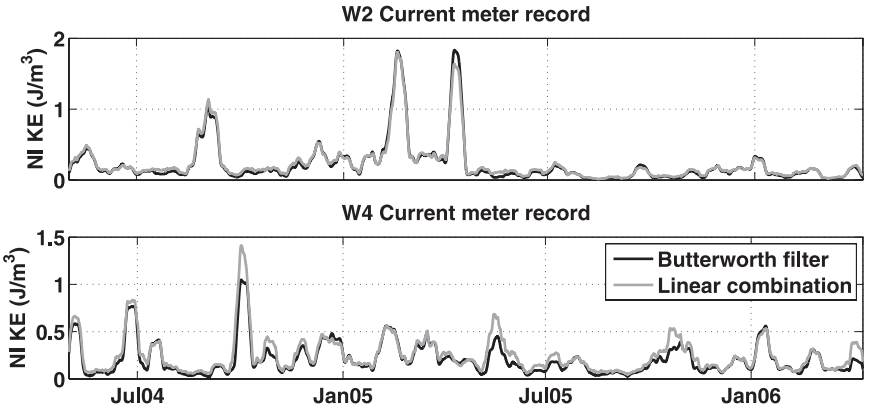

FIG. A1. Comparison of the subsampling inertial-filter technique with a Butterworth inertial-filter technique applied to Line W vector averaging current meter (VACM) records. The records were averaged over an 11-day period for comparison purposes.

because near-inertial motions are very nearly circularly polarized, and the velocity components are 90° out of phase, calculation of the near-inertial kinetic energy as in Eq. (2) is only weakly dependent on the phase.

To quantify the efficacy of this near-inertial filtering scheme, current meter data from two Line W moorings were examined. The W2 and W4 moorings were located at (39.2°N, 69.4°W) and (38.4°N, 68.9°W), respectively, and both supported vector averaging current meters at 1000-m depth that recorded at half-hour temporal resolution. Data taken from the time period spanning April 2004–April 2006 were subsampled at half inertial period increments (9.5 h) in order to mimic the MMP sampling scheme. The linear combination inertial filtering scheme was then applied to the subsampled current meter records to obtain near-inertial zonal and meridional velocities, and the near-inertial kinetic energy was calculated using Eq. (2). The full current meter records were also filtered using a Butterworth filter with a pass window of 4.5–6 $\times 10^{-2}$ cph (which corresponds to $0.85f$–$1.15f$ at the latitude of the moorings). A near-inertial kinetic energy time series was calculated for these filtered velocity records and was compared to the subsampled filtered kinetic energy (Fig. A1). It can be seen that the linear combination filtering technique accurately captures the magnitude and basic temporal evolution of the near-inertial kinetic energy. The frequency response of the filter was also estimated by comparing the kinetic energy spectrum of the full W4 current meter record and the kinetic energy spectrum of the same current meter record with the linear combination filter applied (Fig. A2). The linear combination filter passed 98% of the energy in the near-inertial frequency band and just 3% of the energy in the semidiurnal tidal band (defined here as 7–9 x 10^{-2} cph). Equations (1) and (2) were therefore applied to the MMP measurements to estimate near-inertial kinetic energy time series.

APPENDIX B

Estimation of the Wind Work on Near-Inertial Motions

For this study, the wind work on inertial motions was calculated as the dot product of the near-inertial surface currents with the near-inertial wind stress. Studies that

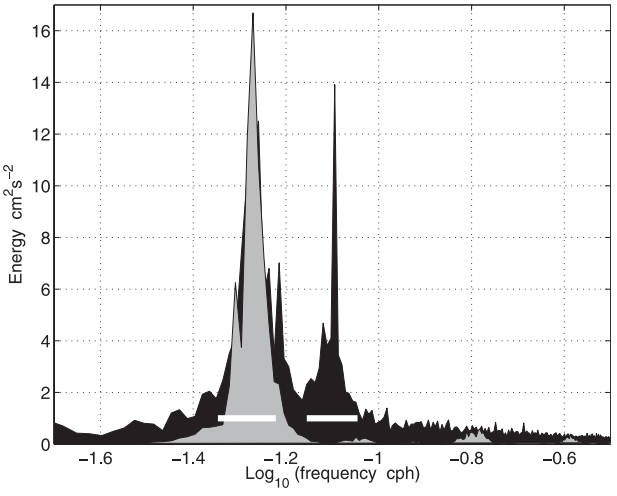

FIG. A2. Semilog plot of the kinetic energy spectrum of the full W4 current meter record (black) and the near-inertial kinetic energy estimated using the linear combination filter (gray). The white horizontal lines represent the extent of the (left) near-inertial and (right) semidiurnal frequency bands. The spectra represent the average of 25 periodograms estimated from successive 28-day segments of the current meter record.

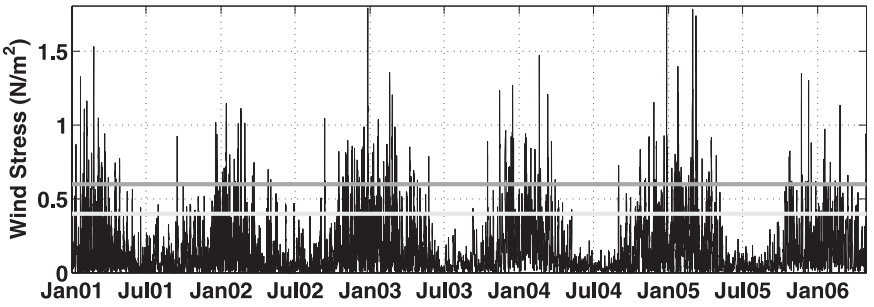

FIG. B1. Time series of the wind stress calculated from the spliced NBDC buoy and NCEP–NCAR reanalysis data. The light gray line represents the 0.4 N m^{-2} reinitialization criteria and the dark gray line represents the 0.6 N m^{-2} reinitialization criteria used for the PWP model runs.

have used a mixed layer kinetic energy budget to study wind forcing often use a different formula to estimate the wind work in which the wind work is dependent on the time derivative of the wind stress (D'Asaro 1985; Plueddemann and Farrar 2006). Analysis done for this study demonstrated that the differences between the two formulations are small and do not affect the conclusions of this paper.

Meteorological surface data were acquired from National Data Buoy Center (NDBC) buoy 44004 (information online at www.ndbc.noaa.gov), which is located at 38.5°N and 70.4°W, approximately 116 km from the MMP moorings (Fig. 2). There was a period of time when the buoy data were unavailable; during this interval, which totaled approximately 15 months out of the 5.5-yr analysis period, National Centers for Environmental Prediction–National Center for Atmospheric Research (NCEP–NCAR) reanalysis data (Kalnay et al. 1996) were interpolated to the NDBC buoy site and used in a similar fashion as the NDBC data. Comparison between the NDBC buoy data and NCEP–NCAR reanalysis data at times when they were both available showed them to be in reasonable agreement.

Because of the distance between the NDBC buoy and MMP mooring locations, as well as the fact that the MMP moorings did not sample the surface mixed layer currents continuously, the PWP model was invoked to estimate the mixed layer near-inertial currents. Hourly sampled NDBC buoy (or NCEP–NCAR fields when the buoy was not operating) air temperature, wind direction and speed, atmospheric pressure, dewpoint temperature, and sea surface temperature were used to estimate a wind stress time series and the buoyancy forcing time series needed to drive the PWP model. The Couple Ocean–Atmosphere Response Experiment (COARE) bulk air–sea flux algorithm was utilized to estimate the wind stress and the sensible and latent heat fluxes from the spliced NDBC and NCEP–NCAR reanalysis data (Fairall et al. 1996). Longwave and solar heat fluxes were obtained strictly from the NCEP–NCAR reanalysis data. The freshwater flux was neglected for the PWP runs.

Because PWP is a one-dimensional mixed layer model and does not include terms such as advection, etc., it is necessary to reinitialize it occasionally in order to ensure that the model stratification remains close to the observed. Most of the wind energy input into inertial motions occurs early (in a fraction of an inertial period) within intense wind events. Between such events, the phase relationship between surface currents and the wind tends to be random (incurring little net energy input). With this in mind, a reinitialization scheme based on the wind stress magnitude was implemented. The model was reinitialized approximately one inertial period (19 h) after the peak of strong wind events in which the wind stress magnitude surpassed a set threshold. Model reinitialization involved resetting the density to the observed density profile, and the model velocity profiles to zero. The reinitialization scheme was run for two wind stress thresholds: 0.4 and 0.6 N m^{-2} (Fig. B1). The mean wintertime wind stress calculated from NDBC buoy and NCEP–NCAR reanalysis data was 0.24 N m^{-2}, with wintertime wind stress peaks reaching 1 N m^{-2}.

To investigate the sensitivity of the wind work results to the PWP reinitialization scheme used, two additional PWP model runs were carried out. The first involved reinitializing the model on a monthly basis, with no dependence on wind stress, and the second initialized the model before strong (>0.6 N m^{-2}) wind events (as opposed to after). It was found that the wind work time series calculated from all four of these model runs are similar in character, with the wind stress criteria based model runs being comparable in magnitude as well. The monthly reinitialized model run results in an estimate for the time-averaged wind work that is smaller than that predicted from the other model runs by about 25%. Therefore, it was concluded that the results were not

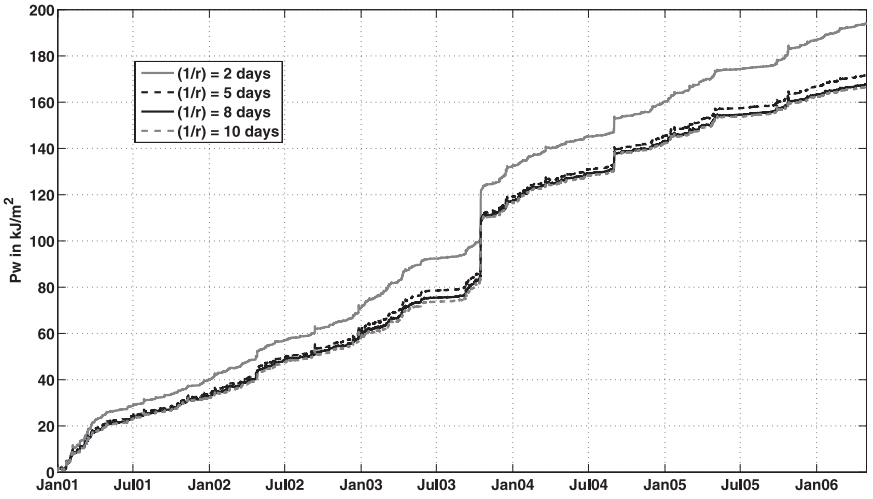

FIG. B2. Time-integrated wind work for varying values of the dissipation coefficient r.

particularly sensitive to the reinitialization scheme, and ultimately the PWP run that was reinitialized after major wind events with a wind stress threshold of 0.6 N m^{-2} was adopted.

In addition to wind stress and buoyancy flux time series, the PWP model requires density profile data for the reinitializations, which came from the MMP temperature and salinity data. Because the MMP measurements did not span the whole water column, it was necessary to extend the observed density profiles to the surface. Some of the MMP density profiles (particularly in winter) reached into the surface mixed layer; in these instances the temperature and salinity were extrapolated upward to the surface as constant values. Whenever the MMP did not reach into the mixed layer, NDBC SST data were used to interpolate the temperature profile by linearly extrapolating the MMP temperature profile up from the shallowest sampled levels to the observed SST value, and assuming constant values above. Mixed layer depth was then calculated from the interpolated temperature profile. The MMP salinity profile was linearly extrapolated up to the inferred mixed layer depth and assumed constant above, thus allowing for the calculation of the density. If at the time of a reinitialization the SST was unknown and the MMP measurements did not reach into the mixed layer, the current PWP model density profile was retained. The PWP model was run with an hourly time step spanning the period from fall 2001 to spring 2006. The model-derived surface velocity and wind stress were subsequently filtered about the inertial frequency using a running boxcar technique with a pass window of $0.5f$–$2f$ before calculating the wind energy input into inertial motions using (4).

The PWP model runs were carried out with a linear drag parameterization as in Plueddemann and Farrar (2006). This drag term represents exchanges of momentum and energy between the base of the modeled layer and the ocean below beyond those associated with mixing in the transition layer. The lack of surface velocity observations in this region precluded attempts to tune the damping coefficient r to match the PWP surface velocities to the observations. Therefore, a set of varying r values was tested to determine the kinetic energy model's sensitivity to the damping coefficient.

The wind work input into inertial motions was evaluated in the form of a time integral of the wind work term ($P_w = \int \mathbf{u}_i \cdot \boldsymbol{\tau}_i dt$) (Fig. B2). The seasonal cycle of the wind work on inertial motions can be seen as a wintertime increase of the slope of P_w as compared to the summertime. The mean wintertime (December–February) wind work is 1.1 mW m^{-2}, which is 2 times larger than the summertime (June–August) mean of 0.55 mW m^{-2}. Varying the damping coefficient for the PWP model made very little difference to the shape or magnitude of the estimated work done by the wind on inertial motions. Therefore, the intermediate value of $(1/r) = 5.7$ days, as suggested in Plueddemann and Farrar (2006), was chosen for the implementation of the kinetic energy model.

REFERENCES

Alford, M. H., 2001: Internal swell generation: The spatial distribution of energy flux from the wind to mixed layer near-inertial motions. *J. Phys. Oceanogr.,* **31,** 2359–2368.

——, 2003: Improved global maps and 54-year history of wind-work on ocean inertial motions. *Geophys. Res. Lett.,* **30,** 1424, doi:10.1029/2002GL016614.

——, and M. Whitmont, 2007: Seasonal and spatial variability of near-inertial kinetic energy from historical mooring velocity records. *J. Phys. Oceanogr.,* **37,** 2022–2037.

D'Asaro, E. A., 1985: The energy flux from the wind to near-inertial motions in the surface mixed layer. *J. Phys. Oceanogr.,* **15,** 1043–1059.

——, C. C. Eriksen, M. D. Levine, P. Niiler, C. A. Paulson, and P. Van Meurs, 1995: Upper ocean inertial currents forced by a strong storm. Part I: Data and comparisons with linear theory. *J. Phys. Oceanogr.,* **25,** 2909–2936.

Doherty, K. W., D. E. Frye, S. P. Liberatore, and J. M. Toole, 1999: A moored profiling instrument. *J. Atmos. Oceanic Technol.,* **16,** 1816–1829.

Fairall, C. W., E. F. Bradley, D. P. Rogers, J. B. Edson, and G. S. Young, 1996: Bulk parameterization of air–sea fluxes for Tropical Ocean Global Atmosphere Coupled Ocean–Atmosphere Response Experiment. *J. Geophys. Res.,* **101,** 3747–3764.

Garrett, C., 2001: What is the ''near-inertial'' band and why is it different from the rest of the internal wave spectrum? *J. Phys. Oceanogr.,* **31,** 962–971.

Gregg, M. C., 1989: Scaling turbulent dissipation in the thermocline. *J. Geophys. Res.,* **94,** 9686–9698.

Henyey, F. S., J. Wright, and S. M. Flatte, 1986: Energy and action flow through the internal wave field: An eikonal approach. *J. Geophys. Res.,* **91,** 8487–8495.

Kalnay, E., and Coauthors, 1996: The NCEP/NCAR 40-Year Reanalysis Project. *Bull. Amer. Meteor. Soc.,* **77,** 437–470.

Kunze, E., R. W. Schmitt, and J. M. Toole, 1995: The energy balance in a warm-core ring's near-inertial critical layer. *J. Phys. Oceanogr.,* **25,** 942–957.

Leaman, K. D., and T. B. Sanford, 1975: Vertical energy propagation of inertial waves: A vector spectral analysis of velocity profiles. *J. Geophys. Res.,* **80,** 1975–1978.

McComas, C. H., and P. Muller, 1981: The dynamic balance of internal waves. *J. Phys. Oceanogr.,* **11,** 970–986.

Morrison, A. T., III, J. D. Billings, and K. W. Doherty, 2000: The McLane moored profiler: An autonomous platform for oceanographic measurements. *Proc. Oceans 2000*, Vol. 1, Providence, RI, IEEE, 353–358.

Munk, W., 1981: Internal waves and small-scale processes. *Evolution of Physical Oceanography*, B. A. Warren and C. Wunsch, Eds., The MIT Press, 264–291.

——, and C. Wunsch, 1998: Abyssal recipes II: Energetics of tidal and wind mixing. *Deep-Sea Res. I,* **45,** 1977–2010.

Plueddemann, A. J., and J. T. Farrar, 2006: Observations and models of the energy flux from the wind to mixed-layer inertial currents. *Deep-Sea Res. II,* **53,** 5–30.

Pollard, R. T., and R. C. Millard, 1970: Comparison between observed and simulated wind-generated inertial oscillations. *Deep-Sea Res.,* **17,** 153–175.

Polzin, K. L., J. M. Toole, and R. W. Schmitt, 1995: Finescale parameterizations of turbulent dissipation. *J. Phys. Oceanogr.,* **25,** 306–328.

Price, J. F., R. A. Weller, and R. Pinkel, 1986: Diurnal cycling: Observations and models of the upper ocean response to diurnal heating, cooling, and wind mixing. *J. Geophys. Res.,* **91,** 8411–8427.

Skyllingstad, E. D., W. D. Smyth, and G. B. Crawford, 2000: Resonant wind driven mixing in the ocean boundary layer. *J. Phys. Oceanogr.,* **30,** 1866–1890.

Toole, J. M., K. W. Doherty, D. E. Frye, and S. P. Liberatore, 1999: Velocity measurements from a moored profiling instrument. *Proc. Sixth Working Conf. on Current Measurement*, San Diego, CA, IEEE, 144–149.